# Maastricht University

# Effect of ultrasound on bone fracture healing

**Please check the document version of this publication:**

• A submitted manuscript is the version of the article upon submission and before peer-review. There can
be important differences between the submitted version and the official published version of record.
People interested in the research are advised to contact the author for the final version of the publication,
or visit the DOI to the publisher's website.
• The final author version and the galley proof are versions of the publication after peer review.
• The final published version features the final layout of the paper including the volume, issue and page
numbers.

Link to publication

# Effect of ultrasound on bone fracture healing: A computational mechanobioregulatory model

Konstantinos N. Grivas,[1] Maria G. Vavva,[1] Demosthenes Polyzos,[1] Aurélie Carlier,[2]
Liesbet Geris,[2] Hans Van Oosterwyck,[2] and Dimitrios I. Fotiadis[3,a)]

[1]*Department of Mechanical Engineering and Aeronautics, University of Patras, GR 26500, Patras, Greece*
[2]*Department of Mechanical Engineering, KU Leuven, Celestijnenlaan 300C—PB 2419, B-3001, Leuven, Belgium*
[3]*Department of Materials Science and Engineering, University of Ioannina, GR 45110, Ioannina, Greece*

Bone healing process is a complicated phenomenon regulated by biochemical and mechanical signals. Experimental studies have shown that ultrasound (US) accelerates bone ossification and has a multiple influence on cell differentiation and angiogenesis. In a recent work of the authors, a bioregulatory model for providing bone-healing predictions was addressed, taking into account for the first time the salutary effect of US on the involved angiogenesis. In the present work, a mechanobioregulatory model of bone solidification under the US presence incorporating also the mechanical environment on the regeneration process, which is known to affect cellular processes, is presented. An iterative procedure is adopted, where the finite element method is employed to compute the mechanical stimuli at the linear elastic phases of the poroelastic callus region and a coupled system of partial differential equations to simulate the enhancement by the US cell angiogenesis process and thus the oxygen concentration in the fractured area. Numerical simulations with and without the presence of US that illustrate the influence of progenitor cells' origin in the healing pattern and the healing rate and simultaneously demonstrate the salutary effect of US on bone repair are presented and discussed. © 2019 Acoustical Society of America. https://doi.org/10.1121/1.5089221

## I. INTRODUCTION

Secondary bone healing is a complex procedure taking place in four stages, i.e., the inflammatory, callus differentiation, ossification, and bone remodeling stages, all characterized by biochemical signals, mechanical stimuli, and a plethora of other impressive cellular and molecular processes.

During the last three decades, several mathematical models and computational methods have been proposed to simulate the difficult procedure of secondary bone healing (Betts and Müller, 2014; Wang *et al.*, 2017; Ghiasi *et al.*, 2017). Although more intensive work is required on the subject, these models offer a powerful tool that helps scientists and practitioners to elucidate underlying mechanisms, explore the involved complex biological processes, test bone healing acceleration scenarios, and optimize treatment techniques (Pivonka and Dunstan, 2012). Besides, the use of those computational models allows one to perform easily and economically many parametric studies, which otherwise would require expensive and time-consuming *in vivo* and *in vitro* experiments to be conducted.

As it is mentioned in the very recent review work of Wang *et al.* (2017), all the relevant mathematical and computational models proposed so far in the literature can be grouped into three categories. The first category concerns the bioregulatory models like the one demonstrated in the recent work of Vavva *et al.* (2018). In this category, the

biochemical factors involved in cell signaling and differentiation are only considered in bone healing simulations. The second category deals with the so-called mechanoregulatory models, where the mechanical stimuli possess the key-role of bone healing. Finally, in the third category belong the coupled mechanobioregulatory models that effectively combine the models mentioned in the previous two categories.

Focusing on mechanoregulatory and mechanobioregulatory models, it is well known that successful healing requires the stabilization of the bone using applicable forces on it. First, Pauwels (1941) reported that pseudarthrosis occurs when the fractured bone is inadequately fixed. Many years later, Pauwels (1960) presented the exact parameters and the mechanical environment that exist to achieve bone formation. Distortional stress affects the development of fibrous connective tissue and hydrostatic compression stimulates cartilage formation. Furthermore, experimental (Augat *et al.*, 1998; Claes *et al.*, 1998) and clinical studies (Goodship and Kenwright, 1985; Goodship *et al.*, 1998; Kenwright and Gardner, 1998) have demonstrated that mechanical loading plays a significant role in bone fracture healing.

During the last decades numerous mechanoregulation and mechanobioregulation computational models have appeared to demonstrate the relationship between mechanical loading and tissue differentiation, especially in bone healing (Ament and Hofer, 2000; Carter *et al.*, 1998; Claes and Heigele, 1999; Prendergast, 1997; Alierta *et al.*, 2014; Vetter *et al.*, 2012, Wang *et al.*, 2017; Ghiasi *et al.*, 2017; Wilson *et al.*, 2017). Several mechanical loadings have been

a)Electronic mail: fotiadis@cc.uoi.gr

investigated which mainly include force application at the boundary, force transmission through the tissue matrix, mechanosensation and transduction by cells, and transformation of the extracellular matrix characteristics (Isaksson *et al.*, 2011a, 2011b).

Lacroix *et al.* (2002) used a diffusion equation to model the concentration of progenitor cells through proliferation, originating from the periosteum, the bone marrow, as well as the soft tissue external to the callus. In this approach, progenitor cells were considered to differentiate into fibroblasts, chondrocytes, or osteoblasts, following a mechanoregulation concept, which will be explained in detail later. Bailon-Plaza and van der Meulen (2001) focused on the cell and molecular mechanisms of the bone healing while Perez and Prendergast (2007) introduced a stochastic model of cell dissemination into the mechanoregulation algorithm. Garcia-Aznar *et al.* (2007) and Gomez-Benito *et al.* (2005) have suggested a model of tissue differentiation, which considers cellular processes along with volumetric tissue growth.

Researchers have recently developed computational models incorporating other significant determinants of bone healing apart from the mechanical environment, such as angiogenesis and/or the nutrient supply in directing tissue differentiation within a fracture callus (Chen *et al.*, 2009; Checa and Prendergast, 2009; Carlier *et al.*, 2015; Geris *et al.*, 2010a; Shefelbine *et al.*, 2005). In more detail, Geris *et al.* (2008) developed a continuous mechanical model using a number of partial differential equations to describe the bone-healing phenomenon. The healing process, using this method, was found to be in agreement with experimental observations. Later on, the authors extended their previous study in order to take into account the effect of mechanical stimulus in their model (Geris *et al.*, 2010b). Finally, OReilly *et al.* (2016) employed a computational mechanobiological model to examine whether the local oxygen tension regulates chondrocyte hypertrophy and endochondral ossification of the cartilaginous matrix within the callus of a fractured long bone. To this goal they set up a three-dimensional Finite Element Method (FEM) model of the fracture callus to determine the biophysical stimuli generated by the loading of the callus during gait.

In the present work, a new FEM computational mechanobioregulatory model is proposed. More precisely, the computational model for tissue differentiation of Checa and Prendergast (2009) is adopted, with the difference that the vascularization process and thus the supply of oxygen and nutrients to cells is accomplished through the bioregulatory computational model addressed in our recent work (Vavva *et al.*, 2018). In that work, the salutary effect of Low Intensity Pulsed Ultrasound on bone healing is reviewed and is taken into account by introducing, in the considered system of equations, a term associated with the diffusion of ultrasound (US) in the injured area. As explained by Xu *et al.* (2006), fluid saturated porous media subjected to a small amplitude oscillatory pressure gradient appears as micro-fluid flow caused by the imposed pressure fluctuations, a phenomenon that can be described by dynamic diffusion. Such a consideration takes into account the low intensity of the US and the imposed pressure gradient (Qin *et al.*, 2003) than its wave characteristics

like pulse duration and frequency. Investigation on the influence of the wave characteristics of the US on the acceleration of bone fracture healing requires more detailed models where the interaction of US with the different microstructure of the healing phases of the bone has to be considered. However, in this case the US effect is assessed locally (Hosokawa, 2013) rather than globally, as in the case of Vavva *et al.* (2018). Thus, in the present work, the positive influence of US is automatically taken into account via the global bioregulatory model of Vavva *et al.* (2018).

The paper is organized as follows: In Sec. II the materials and the flow chart of the iterative computational process followed in the present work are illustrated and presented in detail. The essential stages of fracture healing process obtained by the simulations along with the influence of US to the speed of healing are demonstrated as well. Finally, the obtained results are analyzed and discussed assiduously in Secs. III and IV.

## II. THE MECHANOBIOREGULATORY MODEL

In the present study, we propose a coupled mechanobioregulatory model for simulating bone fracture healing under US enhancement. That coupled model combines our previous multiscale model (Vavva *et al.*, 2018) and a mechanoregulatory model based on the idea of Checa and Prendergast (2009) of considering tissue differentiation based on the local mechanical environment and the local vascularity. The effect of US in the new model is introduced as vascularization enhancement via an angiogenesis procedure facilitated by the bioregulatory model presented in Vavva *et al.* (2018). The main steps and the underlying iterative process of the proposed model are schematically presented in the flowchart of Fig. 1 and explained in what follows. The bioregulatory and mechanoregulatory parts of the coupled model are indicated in the flowchart by boxes with continuous red and black lines, respectively, while their coupling is depicted with dashed lined boxes.

### A. The bioregulatory part of the coupled model

The bioregulatory part of the coupled mechanobioregulatory model proposed here is that of Vavva *et al.* (2018) and it is employed here just for two specific purposes: first to predict the Mesenchymal Stem Cells (MSCs) migration and proliferation during the healing process and, second, to simulate the spatiotemporal evolution of vasculature under the US effect to determine the oxygen concentration inside the callus.

The calculation of (MSC) concentrations ($c_m$) is derived from the solution of the following non-linear diffusion (Fisher) equation:

$$\frac{\partial c_m}{\partial t} = \nabla \cdot (D_m \nabla c_m - C_{mCT} c_m \nabla (g_b + g_v) - C_{mHT} c_m \nabla_m)$$
$$+ A_m c_m (1 - \alpha_m c_m) - F_1 c_m - F_2 c_m - F_4 c_m, \qquad (1)$$

where the functional forms related to migration ($D_m$, $C_{mCT}$, $C_{mHT}$), proliferation ($A_m$), chondrogenic differentiation ($F_2$), the differentiation of mesenchymal stem cell toward osteoblasts ($F_1$), the differentiation of mesenchymal stem cells into fibroblasts ($F_4$), and the variables for the generic

J. Acoust. Soc. Am. **145** (2), February 2019
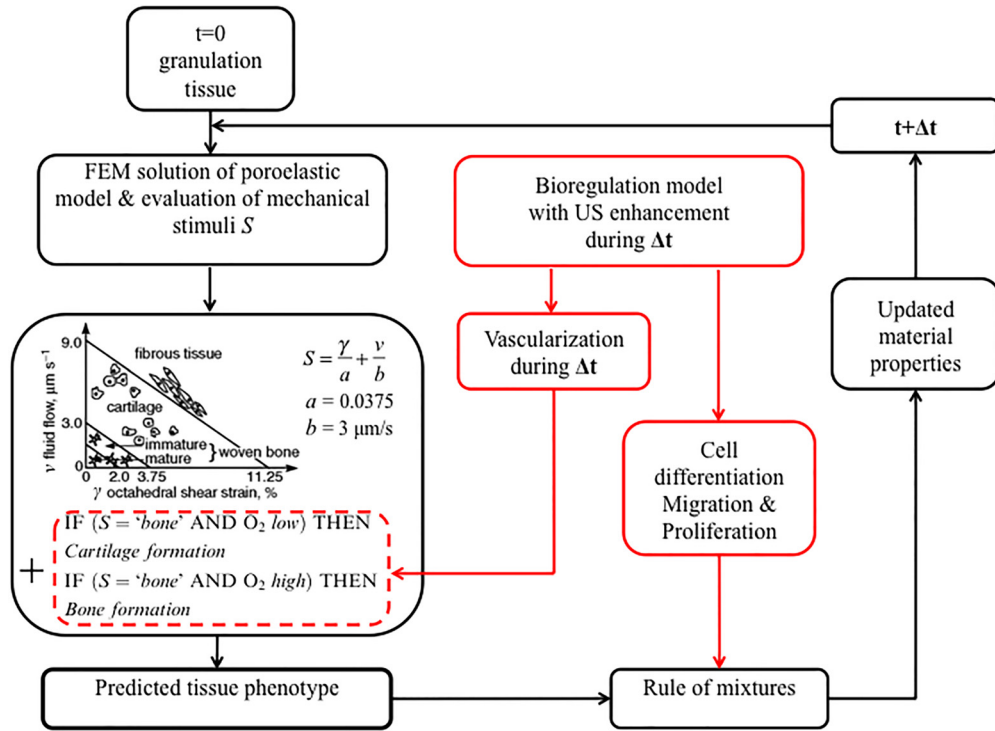
Grivas *et al.* 1049

FIG. 1. (Color online) Flowchart of the iterative coupled mechanobioregulatory model used for tissue regeneration during bone healing. The differentiation process is regulated by the local mechanical environment (biophysical stimuli S) and local vascularity (oxygen concentration).

osteogenic ($g_b$), the generic angiogenic growth factor ($g_v$), and the total matrix density ($m$) influencing the random motion were taken from Geris *et al.* (2008) and $\alpha_m$ is indicated from the limiting densities as described in Bailon-Plaza and van der Meulen (2001).

The above-mentioned formulation is applied to the geometrical domain defined in Fig. 2(a). The results of Eq. (1) are related to the migration and proliferation of the MSCs inside the callus region and they will be used in the rule of mixture, which will be explained later in the present work, as shown in Fig. 1. Concerning the initial conditions, fixed MSC concentrations are assumed on either (i) periosteum layer, (ii) periosteum cortical interface, or (iii) bone marrow interface depending on the assumption for the origin of the cells (see below). To establish how MSCs are

distributed inside the selected geometry 200 iterations were required, which corresponds to 35 days post-fracture healing period.

The spatiotemporal evolution of blood vessels, carrying the oxygen inside the callus, is determined by solving numerically the system of 12 coupled differential equations, addressed in Vavva *et al.* (2018), which describe the spatiotemporal variation of mesenchymal stem cell ($c_m$), fibroblasts ($c_f$), chondrocytes ($c_c$), osteoblasts ($c_b$), fibrous extracellular matrix ($m_f$), cartilaginous extracellular matrix ($m_c$), bone extracellular matrix ($m_b$), generic osteogenic ($g_b$), chondrogenic ($g_c$), and vascular growth factors ($g_v$) as well as the concentration of oxygen and nutrients ($n$). To describe the sprout dynamics the discrete variable $c_v$ is used, while the effect of US on $c_v$ is represented by

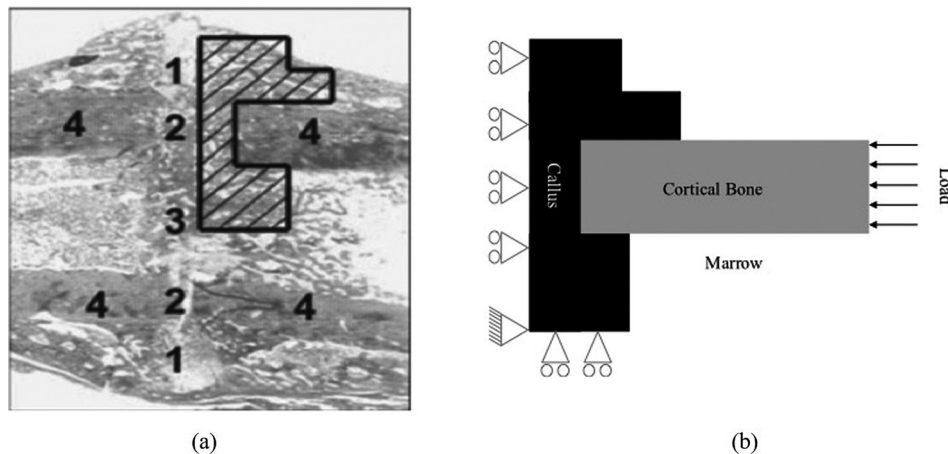

(a)

(b)

FIG. 2. (a) The geometrical domain models one-fourth of the real fracture callus geometry due to reasons of symmetry: (1) periosteal callus; (2) intercortical callus; (3) endosteal callus; and (4) cortical bone ends. (b) Geometrical model of bone fracture for the poroelastic FEM model. The origin of the coordinate system is placed in the left bottom corner of the geometrical domain.
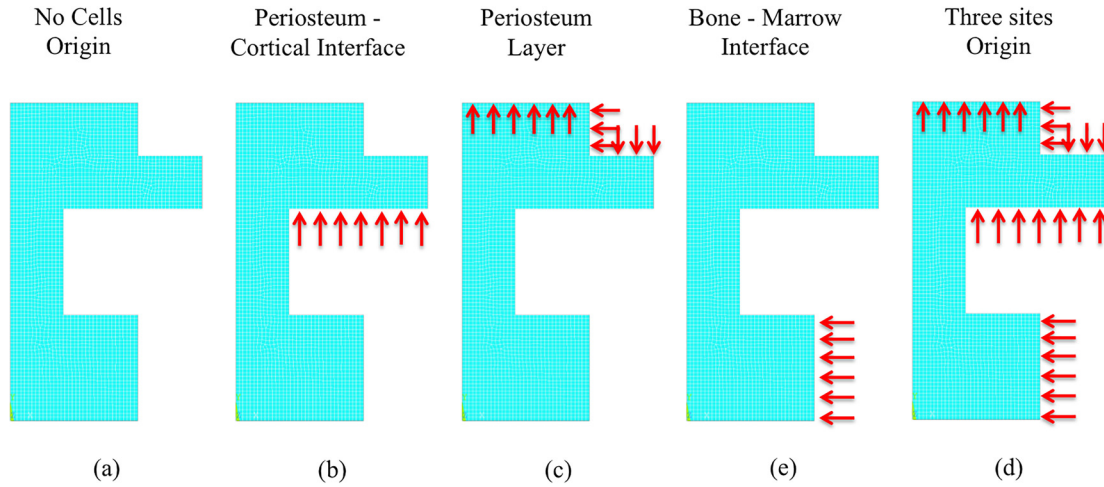
FIG. 3. (Color online) The geometry of the callus along with the different cell origins indicated by the red arrows. (a) No cells origin is considered, (b) cells come from the periosteum-cortical interface, (c) cells originating from the periosteum layer, (d) cells' diffusion takes place from bone-marrow interface, and (e) cells originate from the three previous interfaces.

the US pressure gradient $\nabla p$ in the right-hand side of the equation,

$$\frac{\partial g_v}{\partial t} = \nabla \cdot (D_{gv}\nabla g_v + Kg_v\nabla p) + E_{gvb}c_b + E_{gvc}c_c$$
$$- g_v(d_{gv} + d_{gvc}c_v). \qquad (2)$$

More details concerning the material properties, geometry, and the numerical implementation of the above-mentioned system can be found in Vavva et al. (2018).

## B. The mechanoregulatory part of the coupled model

After the determination of all necessary biological parameters (MSC and $O_2$ concentration), a FEM model for solving poroelastic problems is employed to determine the shear strain environment and the fluid/solid velocity at the different ossification stages of the bone. A spatial domain [Fig. 2(a)] from real callus geometry, at 3 weeks post fracture in a standardized femoral rat fracture model (Peiffer et al., 2011; Harrison et al., 2003) is employed for the FEM analysis. Due to reasons of symmetry only one-fourth of the considered cross-section is discretized. For compatibility reasons the geometry of the discretized area is the same with the corresponding one used in the bioregulatory model of Vavva et al. (2018). The FEM calculations were performed with the aid of ANSYS Simulation Software (ANSYS Student Release v. 16.2) in a typical PC (Intel® Core™

i7–8650U CPU @ 1.90 GHz, 8.00 GB RAM) with time simulation ranging from 5 to 15 min.

The deduced geometrical domain, which was used for the numerical simulations, can be seen in Fig. 2(b). It consists of three regions, i.e., cortical bone, marrow, and callus. The last is the region of interest in which we examined tissue differentiation during the bone healing process. The gap size was chosen in accordance with the experimental observations of Harrison et al. (2003) who reported the formation of a pseudarthrosis in a 3 mm distracted mid-diaphyseal rat femoral osteotomy. This value is also in the same range as other rat femoral critical defect sizes reported in literature: 1 cm (Vogelin et al., 2005), 8 mm (Tolli et al., 2011), and 6 mm (Drosse et al., 2008).

The cortical bone was subjected to an axial ramp loading of 500 N. The nodes in the transverse plane through the center of fracture were constrained on the longitudinal direction, while the nodes on the centerline of the medullary canal were constrained on the transverse direction. A plane strain mesh was created for the modeling purposes at hand. The mesh had 2733 two-dimensional eight noded-coupled pore-pressure elements (CPT213) and 8516 nodes.

In the analysis of the fracture callus, the origin of the progenitor mesenchymal cells was modeled by a fixed cell concentration being defined on either (i) periosteum layer, (ii) periosteum cortical interface, or (iii) bone marrow interface. Apart from these three cases we examined the combined effect of the three sites origin as well as the no-cells origin case as it is shown in Fig. 3.

TABLE I. Material properties for the different stages in callus formation.

|  | Granulation Tissue | Fibrous Tissue | Cartilage | Immature Bone | Mature Bone | Cortical Bone |
|---|---|---|---|---|---|---|
| Young's modulus (MPa) | 0.2 | 2 | 10 | 1000 | 6000 | 20000 |
| Permeability (m⁴/Ns) | $1 \times 10^{-14}$ | $1 \times 10^{-14}$ | $5 \times 10^{-15}$ | $1 \times 10^{-13}$ | $3.7 \times 10^{-13}$ | $1 \times 10^{-17}$ |
| Poisson's ratio | 0.1667 | 0.1667 | 0.1667 | 0.3 | 0.3 | 0.3 |
| Solid compression modulus (MPa) | 2300 | 2300 | 3400 | 13 920 | 13 920 | 13 920 |
| Fluid compression modulus (MPa) | 2300 | 2300 | 2300 | 2300 | 2300 | 2300 |
| Porosity | 0.8 | 0.8 | 0.8 | 0.8 | 0.8 | 0.04 |

J. Acoust. Soc. Am. **145** (2), February 2019

Grivas et al. 1051
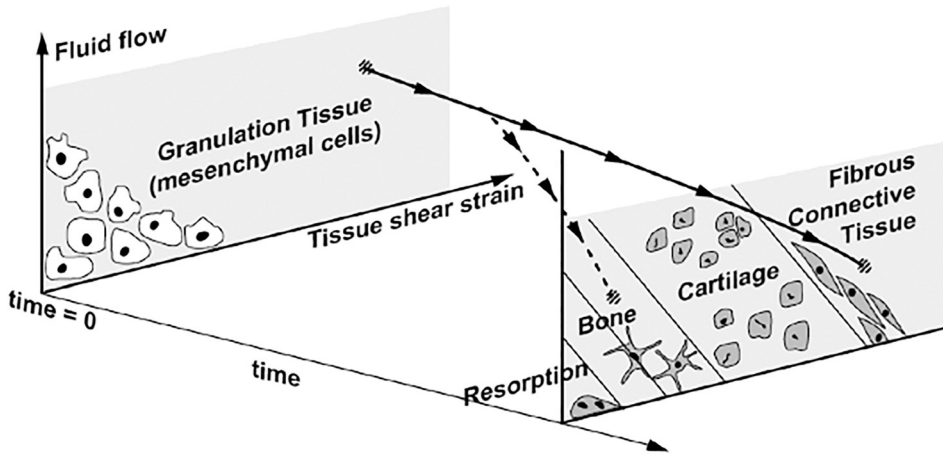
The proliferation coefficients were estimated by considering that a steady state concentration would be reached in the granulation tissue. This gave a proliferation coefficient of $0.1\,\mathrm{mm}^2$/day for the bone marrow site, $0.5\,\mathrm{mm}^2$/day for the periosteum bone interface, and $0.3\,\mathrm{mm}^2$/day for the periosteum layer (Lacroix et al., 2002). Cell concentration was calculated, and the differentiation scheme was implemented to predict tissue phenotype forming every day of the healing period.

The three regions in the fracture site are assigned with material properties equal to cortical bone, bone marrow, and granulation tissue. As healing proceeds, granulation tissue progressively evolves to fibrous tissue, cartilage, and woven bone. Two types of woven bone were modeled representing different stages of maturation, i.e., immature and mature bone. Table I lists the mechanical properties considered for the different tissue phenotypes.

In the present paper we adopted the mechanoregulation algorithm proposed by Prendergast (1997) and modified by Checa and Prendergast (2009). Following that concept, the octahedral shear strain $\gamma$ in the solid phase and the fluid velocity $v$ in the interstitial fluid phase are used as regulators of the tissue differentiation process according to the following equation:

$$S = \frac{\gamma}{a} + \frac{v}{b}, \tag{3}$$

where $S$ is a mechanoregulatory stimulus and $a$, $b$ constants derived empirically for each tissue type. The present work following the suggestions of Prendergast (1997) and Checa and Prendergast (2009) considers $a = 0.0375$ (%), $b = 3\,\mu m/s$.

The diagram of Fig. 4 (Prendergast, 1997) with the limits of the various fields given in Table II, is employed to determine whether the precursor cells would differentiate

into either fibroblasts, chondrocytes, or osteoblasts, leading to the formation of fibrous tissue, cartilaginous tissue, or osseous tissue, respectively. Furthermore, the bone field region was divided into an immature and mature woven bone to represent two mineralization stages of bone formation.

Indicating the role of US in angiogenesis and especially in the growth of blood vessel network inside the callus it is crucial to include the influence of vascularity on tissue differentiation process. Checa and Prendergast (2009) extended Prendergast's algorithm stating that at low mechanical stimuli cartilage will form if there are no blood vessels within a distance from the differentiating cell. This is summarized in the following set of rules:

- IF (S = bone AND $O_2$ = low) THEN Cartilage formation,
- IF (S = bone AND $O_2$ = high) THEN Bone formation,

where no blood vessels surrounding the differentiating cell corresponds to low oxygen concentration ($O_2$ low) and capillaries in the vicinity of the differentiating cell translates into high oxygen concentration ($O_2$ high) and the mechanical stimuli is regulated as shown in Table II (immature and mature bone).

For each iteration, a percentage of MSCs has reached the maturation age and differentiates toward fibroblasts, chondrocytes, or osteoblasts. When MSCs differentiate, a new tissue phenotype is predicted via the mechanoregulation algorithm and the issue of computation of the overall—callus—material properties arises.

In this stage, where two or more different tissue phenotypes exist simultaneously in the finite element model, the rule of mixtures is used to determine the homogenized material properties. In more detail, the MSC concentrations and the maximum concentration at each time step, as calculated in the mechanobiology model (Vavva et al., 2018) is the necessary input data for the considered calculation.

Specifically, the rule for the Young's modulus obtains the form

$$E_{\text{final}} = \frac{C_{\max} - C_{\text{cell}}}{C_{\max}} E_{\text{gran}} + \frac{C_{\text{cell}}}{C_{\max}} E_{\text{upd}}, \tag{4}$$

where $C_{\text{cell}}$ and $C_{\max}$ are the cells' and the maximum concentration in each element of the FEM model, respectively, $E_{\text{upd}}$ is the updated Young's modulus, and $E_{\text{final}}$ is the final value of Young's modulus of the granulation tissue. Similarly, we can calculate the other homogenized mechanical properties such as: permeability, Poisson's ratio, solid, and fluid compression modulus.

TABLE II. The limits of the mechanoregulation algorithm and the corresponding phases in tissue differentiation process.

| | |
|---|---|
| $0.01 < S \le 0.267$ | Stimulation of osteoblasts and maturation of bone (Conditions for mature bone) |
| $0.267 < S \le 1$ | Stimulation of osteoblasts and immature bone (Condition for bone formation) |
| $1 < S < 3$ | Stimulation of chondrocytes and cartilage (Condition for cartilage) |
| $S > 3$ | Stimulation of fibroblasts and fibrous tissue (Condition for fibrous connective tissue) |

## III. RESULTS

The present mechanobioregulatory model captures the essential features of fracture healing phenomenon as they were observed experimentally. Specifically, it begins with the direct differentiation of granulation tissue to bone (intramembranous ossification), predicts the intermediate tissue differentiation phenotypes until the hard callus formation via a cartilage phase (endochondral ossification), and describes quite clearly the bony bridging which signifies the completion of the ossification process. The presence of US and its influence on the speed of healing process is demonstrated and it will be shown that apart from its already proven beneficial effect on angiogenesis it affects significantly the cartilage differentiation accelerating the osseous bridging. Finally, the progenitor cell origin is included in our parametric study since it severely affects the healing pattern and the healing rate as well.

Figures 5–9 represent the ossification predictions estimated for five different cell origins as shown in Fig. 3. For each of the above-mentioned cases, we present two sets of
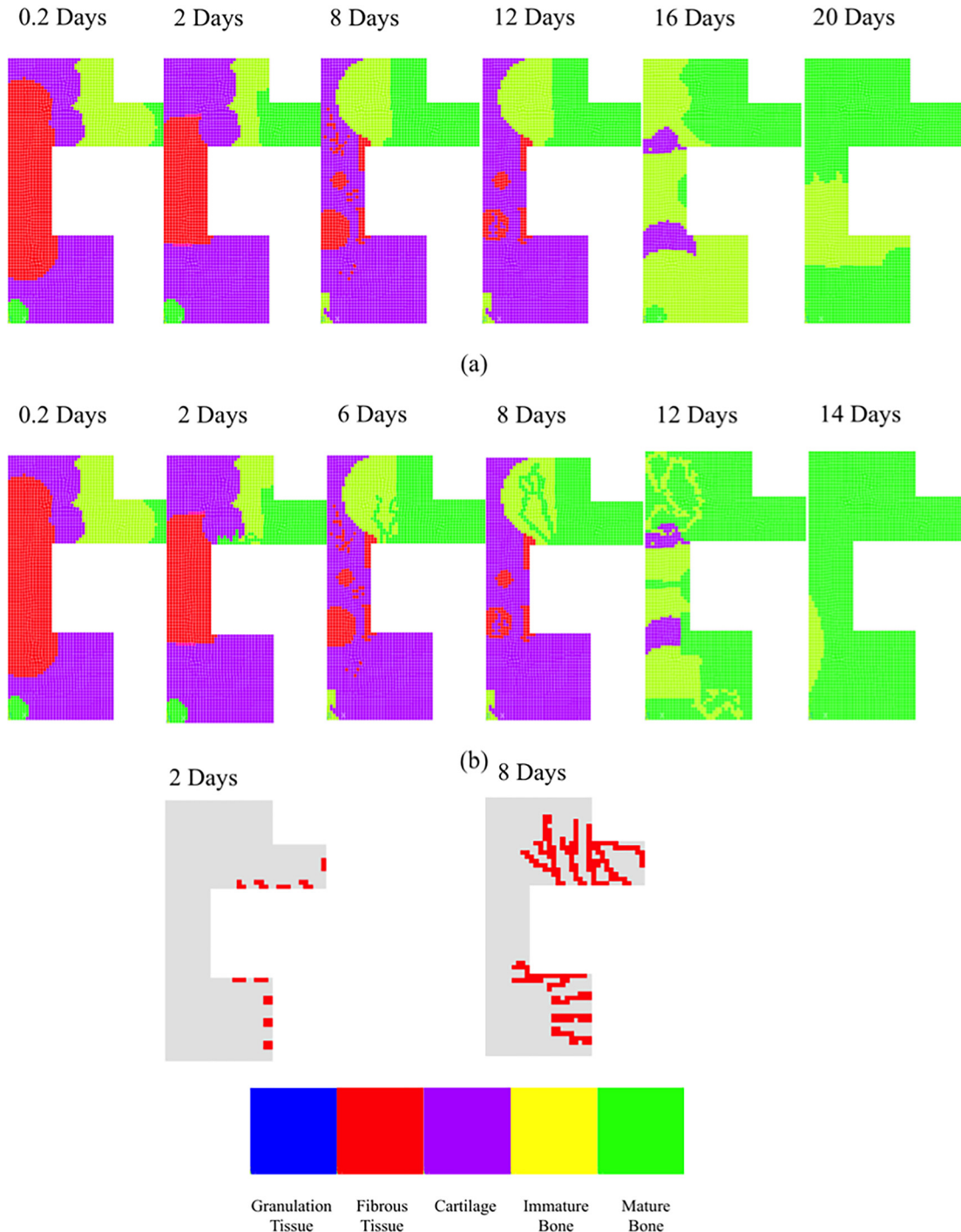


FIG. 5. (Color online) Predicted healing patterns when cells are immediately distributed within the fracture: (a) The analysis was run without including US; and (b) ultrasound effect was taken into consideration. The vascular network from the angiogenesis problem is given at specific days for comparison reasons. The color palette underneath indicates the different tissue phenotypes.

J. Acoust. Soc. Am. **145** (2), February 2019

Grivas *et al.*    1053

FIG. 6. (Color online) Predicted healing patterns when cells originate from the periosteum cortical interface (black arrows): (a) The analysis was run without including US; and (b) ultrasound effect was taken into consideration.

simulations, where the biphasic model under consideration is subjected to a rather high load case of 500 N, with and without the presence of US. To describe as accurately as possible the healing pattern over time, we took into consideration the five tissue phenotypes (granulation tissue, fibrous tissue, cartilage, immature, and mature bone), which were described in detail in Prendergast's mechanoregulatory diagram (Fig. 4).

First, we examine the case where the progenitor cells at $t = 0$ are uniformly distributed within the callus. Based on the sequence shown in Fig. 5(a), we observe that bone formation mainly starts from the periosteal callus. It is found that the region where the direct bone formation takes place is significantly extended and very soon the fracture site is occupied by cartilaginous tissue (12th day). In general, a very rapid ossification process is observed accompanied by a fast evolution of endochondral ossification, which mostly involves the intercortical and endosteal callus regions. Eventually, the differentiation of these regions contributes to the bridging of the fracture gap (16th day) and the completion of the healing process at the 20th day.

When US is imposed in the poroelastic model a quite similar, in quantitative terms, healing pattern occurs. The ossification process is favored in periosteum, but the intramembranous ossification is more intense, and it seems to be enhanced by the growth of the local vascular network. In

more detail, we can see that in the sub-regions where new blood vessels are born, new bone (immature and mature) phenotype is predicted, following the same healing path as it is revealed indicatively by the figures showing the vasculature at days 2 and 8. As healing time passes, the callus region as well as the cortical gap is covered with new bone (12th day) and due to the positive effect of US the ossification process is accelerated significantly lasting only for 14 days, i.e., 30% gain on post-fracture time.

When progenitor cells originate from the periosteum cortical interface [Fig. 3(b)], it is predicted that intramembranous bone formation occurs along the periosteum (external callus). At the second day, some cartilaginous tissue is observed in the external callus and the fracture site mostly constitutes of fibrous tissue. In subsequent days (16th and 20th), cartilaginous tissue is observed at periosteal regions near the fracture gap and in the medullary cavity as well. At this time only small regions of fibrous tissue remain in the fracture gap. Finally, at the 24th day ossification takes place in the callus leading to the bridging of the cortical gap and the gradual replacement of the remaining soft tissues until bone healing is integrated (32nd day). The just described sequence is depicted in Fig. 6(a).

The presence of US [Fig. 6(b)] remains beneficial for the bone healing process as it was noted in the case of Fig. 5. The enhancement of soft callus formation is obvious from
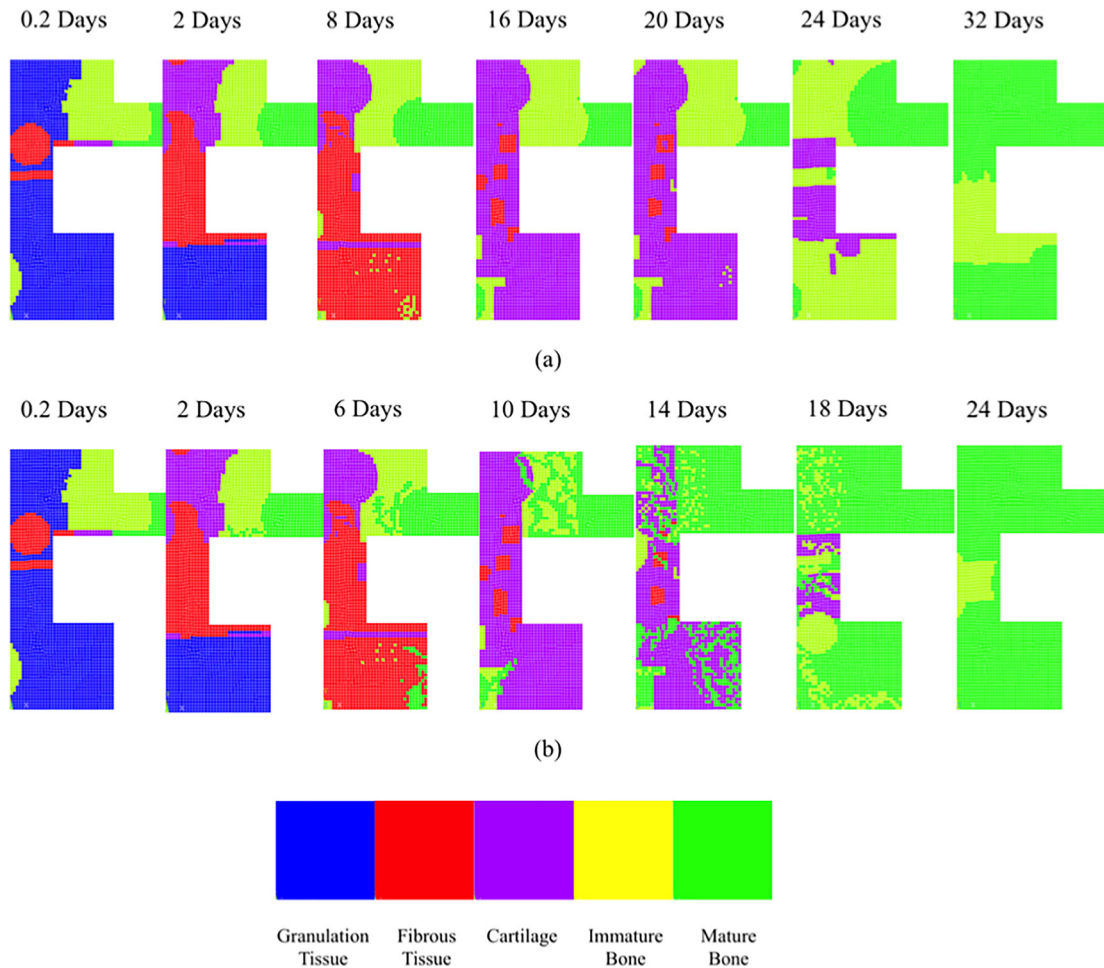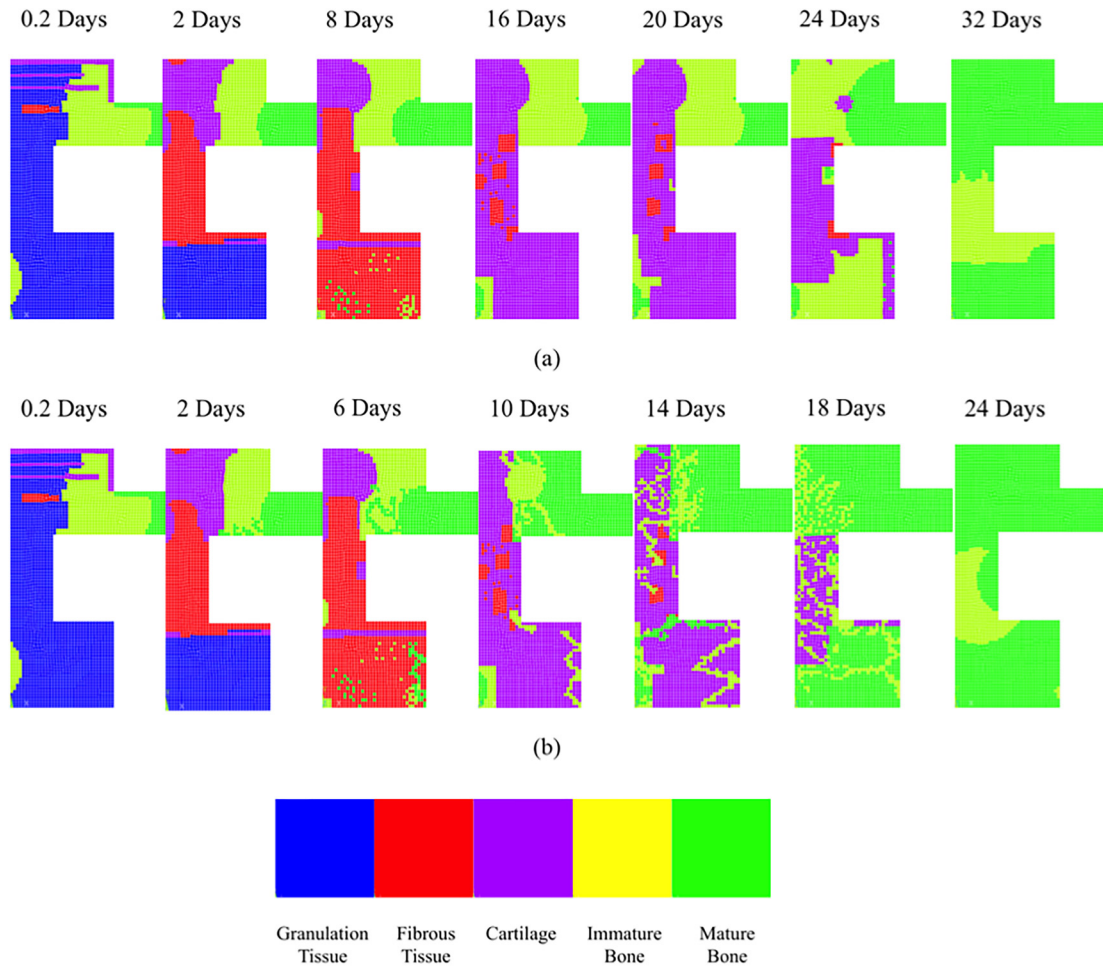
FIG. 7. (Color online) Predicted healing patterns when cells originate from the periosteum layer (black arrows): (a) The analysis was run without including US; and (b) ultrasound effect was taken into consideration.

day 6, when direct bone formation seems to be larger than the respective one in Fig. 6(a). Furthermore, at the 14th day the model predicts two independent ossification fronts (medullary cavity and external callus) progressing at different rates. At this day, bony bridging has already started and endochondral ossification would proceed producing during the next days of simulation mature bone inside the callus region. Consequently, the post fracture time is reduced to 24 days and the healing process under the effect of US becomes 25% faster than in the case of its absence.

When cells originate from the periosteum layer, a similar pattern as the one depicted in Fig. 6(a) is observed, except that the progress of endochondral ossification is much slower as is indicated by the extended regions of cartilage in the fracture gap and the thin zone alongside the bone marrow [24th day; Fig. 7(a)]. Despite the delayed response in hard callus formation, the ossification is completed and bridging in the external callus occurs.

When US is imposed, the healing pattern does not differentiate much from that depicted in Fig. 7(a) at least for the first 6 days. Specifically, until day 10 the transformation of fibrous tissue to cartilage at endosteal regions and in the medullary cavity seems to be the dominant characteristic of the healing process. This transformation is critical for the initiation of endochondral ossification, which will take place in the

subsequent days (14th and 18th days). Although until the 18th day considerable regions of cartilage and immature bone are still observed, US is proven to accelerate the process compared to the case that no US has been employed during the treatment. Ultimately, at the 18th day bridging has already been started and within the next 6 days (the 24th day) the ossification process is completed, reducing the healing period by 25%.

When cells originate from the bone marrow interface, bone formation lasts longer than in previous cases and finally only a small percentage of the callus region has been covered with newly formed bone. As in previous cases the direct bone formation first appears in the external callus. However, the intramembranous ossification process is much more limited, and as a result we observe (2nd day) large regions of undifferentiated tissue in the cortical site. In the following days, fibrous tissue replaces granulation tissue in the cortical region and differentiates to mature bone but the ossification and bridging processes evolve at very slow rates.

Although the ossification process remains slow even in the case of US radiation, Fig. 8(b) reveals a positive contribution of US to bone bridging throughout the medullary canal.

Finally, we examined the case where the progenitor cells originate simultaneously from the above-mentioned three origins (Fig. 9). This case can be considered as the most realistic one since the origination of cells is not focused only

J. Acoust. Soc. Am. **145** (2), February 2019
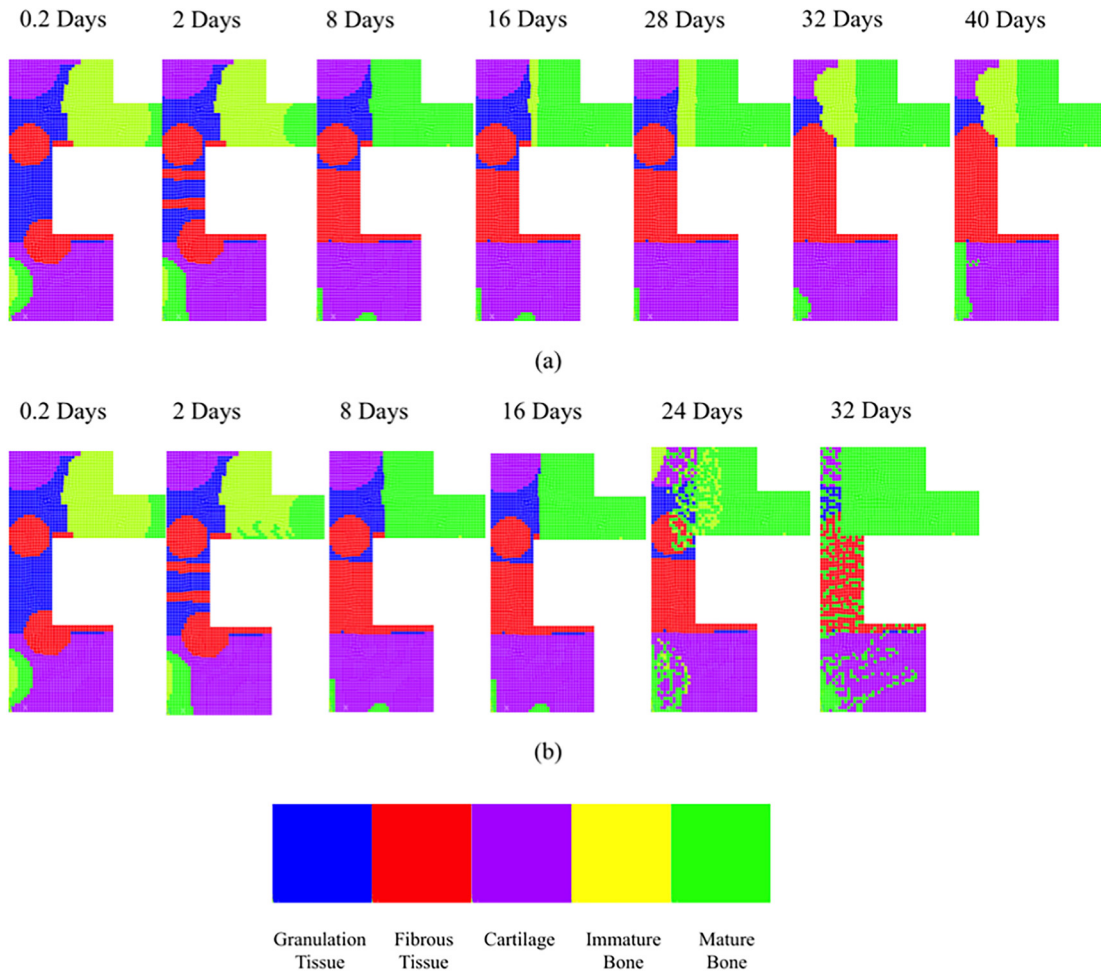
Grivas *et al.* 1055

FIG. 8. (Color online) Predicted healing patterns when cells originate from the bone marrow interface (black arrows): (a) The analysis was run without including US; and (b) ultrasound effect was taken into consideration.

in one region of the formed callus. When US is not included in the poroelastic analysis, the first mechanism associated to the healing process is intramembranous ossification. This process occurs mainly in periosteal regions [8th day; Fig. 9(a)] leaving extended regions of undifferentiated bone elsewhere and more specifically fibrous connective tissue in the fracture gap and cartilage to the remaining areas. Next, endochondral ossification arises in the external callus until stabilization is sufficient to allow osseous bridging at the outside of the callus (32nd day). In the examined case it is clearly seen that new tissue is born through the formation of internal and external callus. This is achieved as a result of the ossification process, which propagates from medullary cavity and external callus (ossification centers) at different rates for each one. Eventually, bone healing is completed at 36 days, namely, 4 days longer than the first two examined scenarios. This is justified due to the fact that we have incorporated into our model much more realistic assumptions (several areas as origins of mesenchymal cells). Moreover, it should be noted that between the two ossification centers, periosteum is predicted to have the main contribution in the differentiation process.

Concerning the simulation where US is taken into consideration, the positive influence of US on the overall process is proven. During the first 6 days intramembranous ossification guides the differentiation but quite soon

endochondral ossification takes the lead and until the 16th day stabilization of endosteal and fracture gap has already been achieved. Thereafter bridging evolves [20th day; Fig. 9(b)] contributing essentially to the fast ossification of the whole callus region (28th day). In total, our model predicts that US accelerates the healing process reducing the post-fracture time by 22%.

## IV. CONCLUSION

In this paper we presented a computational mechano-bioregulation model for predicting the ossification process in bone fracture healing under the presence of US illumination. The models effectively combine the bioregulatory model addressed in our recent work (Vavva et al., 2018) and a mechanoregulatory model that takes into account the influence of vascularization in the bone healing process. The iterative procedure implemented by the present model was based on tissue differentiation taking into account the local mechanical environment and the local vascularity enhanced by the presence of US. More specifically, first we solved the biological problem in order to derive the MSCs concentration at each point of the callus region. Subsequently and separately from the iterative process, the angiogenesis problem has been solved to determine the oxygen concentration
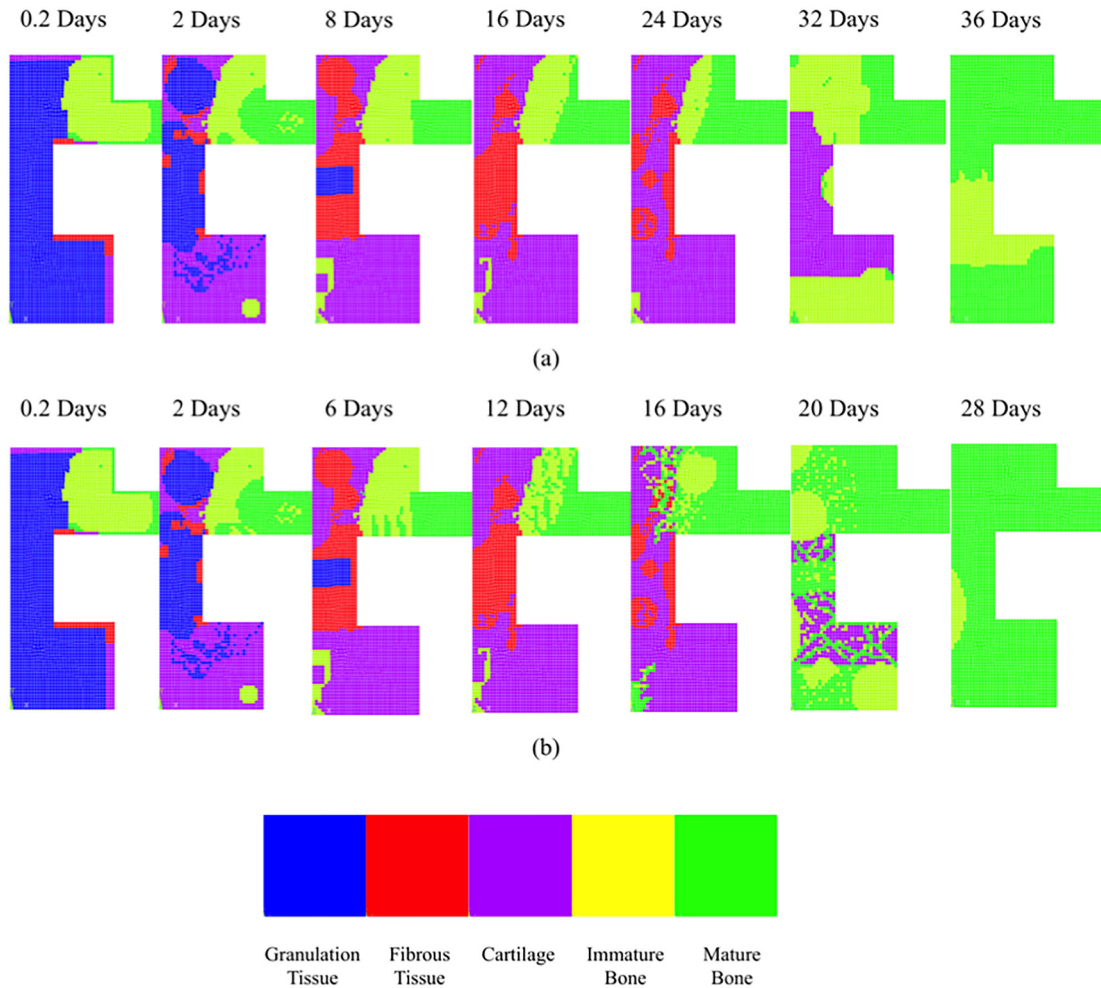
FIG. 9. (Color online) Predicted healing patterns when cells originate from the three origins (black arrows): (a) The analysis was run without including US; and (b) ultrasound effect was taken into consideration.

inside the callus region via the spatiotemporal evolution of the blood vessels network.

The next step of the iterative procedure was to set up the FEM model, which solves the related poroelastic problem and calculates the biophysical stimulus at each point of the callus and at each time step of the iterative algorithm. After the determination of mechanical stimulus (mechanoregulatory model) and oxygen concentration (bioregulatory model) we were able to predict, through Prendergast's mechanoregulation diagram, the occurred tissue phenotype. Several cases of progenitor cell origination have been considered and investigated. The obtained results show that US accelerates first the intramembranous bone ossification, which follows the same healing path with vascular network growth, and second, facilitates the bony bridging which is undoubtedly a core process of endochondral ossification.

The novelty of our model clearly lies at (i) the description of the contribution of US on the vascularization process and subsequently the oxygen concentration in the injured area, and (ii) the consideration of vascularization rate in the FEM iterative procedure applied for the determination of tissue phenotype at all fracture healing stages. Regarding the quality of our numerical results obtained without the presence of US, one can say that they are in good agreement

with the corresponding results provided by other numerical mechanoregulatory models, mentioned in Sec. I. Small differences appearing in the healing time are mainly due to the contribution of the oxygen concentration in the iterations of our FEM model. Our numerical results that take into account the US effect predict a reduction of the post-fracture time by 22%, which seems to be a realistic and conservative result confirming the salutary effect of US in bone healing (Heckman *et al.*, 1994; Kristiansen *et al.*, 1997; Claes and Willie, 2008; Protopappas *et al.*, 2008; de Albornoz *et al.*, 2011; Cheung *et al.*, 2011; Kumagai *et al.*, 2012; Li *et al.*, 2012; Leighton *et al.*, 2017).

We recognize that all predictions provided in the above simulations need to be validated experimentally. Unfortunately, properly designed *in vitro* or *in vivo* experiments that can be used for the validation of a mechanobioregulatory computational model like that proposed here are not available in the literature. As Betts and Müller (2014) mention, the comparison between predictions provided by simulations and experimental studies remains an obstacle for advancing the field. Despite the lack of experimental data for comparisons, the present work successfully takes into account the effect of the diffused pressure field imposed by US in the fractured area and offers a new and reasonable

computational mode, which in conjunction with properly designed experiments is able to give answers to tissue differentiation due to US and solutions to bone fracture treatment and bone scaffolds designing.

## ACKNOWLEDGMENTS

Alierta, J. A., Perez, M. A., and Garcia-Aznar, J. M. (**2014**). "An interface finite element model can be used to predict healing outcome of bone fractures," J. Mech. Behav. Biomed. Mater. **29**, 328–338.

Ament, C., and Hofer, E. P. (**2000**). "A fuzzy logic model of fracture healing," J. Biomech. **33**(8), 961–968.

Augat, P., Margevicius, K., Simon, J., Wolf, S., Suger, G., and Claes, L. (**1998**). "Local tissue properties in bone healing: Influence of size and stability of the osteotomy gap," J. Orthop. Res. **16**(4), 475–481.

Bailon-Plaza, A., and Van der Meulen, C. H. (**2001**). "A mathematical framework to study the effects of growth factor influences on fracture healing," J. Theor. Biol. **212**, 191–209.

Betts, D. C., and Müller, R. (**2014**). "Mechanical regulation of bone regeneration: Theories, models, and experiments," Front. Endocrin. **5**, 1–14.

Carlier, A., Geris, L., Gastel, N. V., Carmeliet, G., and Oosterwyck, H. V. (**2015**). "Oxygen as a critical determinant of bone fracture healing. A multiscale model," J. Theor. Biol. **365**, 247–264.

Carter, D. R., Beaupre, G. S., Giori, N. J., and Helms, J. A. (**1998**). "Mechanobiology of skeletal regeneration," Clin. Orthop. **355S**, S41–S55.

Checa, S., and Prendergast, P. J. (**2009**). "A mechanobiological model for tissue differentiation that includes angiogenesis: A lattice-based modeling approach," Ann. Biomed. Eng. **37**(1), 129–145.

Chen, G., Niemeyer, F., Wehner, T., Simon, U., Schuetz, M. A., Pearcy, M. J., and Claes, L. E. (**2009**). "Simulation of the nutrient supply in fracture healing," J. Biomech. **42**, 2575–2583.

Cheung, W.-H., Chow, S. K.-H., Sun, M.-H., Qin, L., and Leung, K.-S. (**2011**). "Low-intensity pulsed ultrasound accelerated callus formation, angiogenesis and callus remodeling in osteoporotic fracture healing," Ultrasound Med. Biol. **37**(2), 231–238.

Claes, L. E., and Heigele, C. A. (**1999**). "Magnitudes of local stress and strain along bony surfaces predict the course and type of fracture healing," J. Biomech. **32**, 255–266.

Claes, L. E., Heigele, C. A., Neidlinger-Wilke, C., Kaspar, D., Seidl, W., Margevicius, K. J., and Augat, P. (**1998**). "Effects of mechanical factors on the fracture healing process," Clin. Orthop. Rel. Res. **355S**, S132–S147.

Claes, L., and Willie, B. (**2008**). "The enhancement of bone regeneration by ultrasound," Progr. Biophys. Mol. Biol. **93**, 384–398.

de Albornoz, P. M., Khanna, A., Longo, U. G., Forriol, F., and Maffulli, N. (**2011**). "The evidence of low-intensity pulsed ultrasound for in vitro, animal and human fracture healing," British Med. Bull. **100**, 39–57.

Drosse, I., Volkmer, E., Seitz, S., Seitz, H., Penzkofer, R., Zahn, K., Matis, U., Mutschler, W., Augat, P., and Schieker, M. (**2008**). "Validation of a femoral critical size defect model for orthotopic evaluation of bone healing: A biomechanical, veterinary and trauma surgical perspective," Tissue Eng. Part C **14**, 79–88.

Garcia-Aznar, J. M., Kuiper, J. H., Gomez-Benito, M. J., Doblare, M., and Richardson, J. B. (**2007**). "Computational simulation of fracture healing: Influence of interfragmentary movement on the callus growth," J. Biomech. **40**(7), 1467–1476.

Geris, L., Gerisch, A., and Schugart, R. (**2010a**). "Mathematical modeling in wound healing, bone regeneration and tissue engineering," Acta Biotheor. **58**, 355–367.

Geris, L., Schugart, R., and Van Oosterwyck, H. (**2010b**). "In silico design of treatment strategies in wound healing and bone fracture healing," Philos. Trans. Ser. A **368**, 2683–2706.

Geris, L., Vander Sloten, J., and Van Oosterwyck, H. (**2008**). "Angiogenesis in bone fracture healing: A bioregulatory model," J. Theor. Biol. **251**(1), 137–158.

Ghiasi, M. S., Chen, J., Vaziri, A., Rodriguez, E. K., and Nazarian, A. (**2017**). "Bone fracture healing in mechanobiological modeling: A review of principles and methods," Bone Rep. **6**, 87–100.

Gomez-Benito, M. J., Garcıa-Aznar, J. M., Kuiper, J. H., and Doblare, M. (**2005**). "Influence of fracture gap size on the pattern of long bone healing: A computational study," J. Theor. Biol. **235**, 105–119.

Goodship, A. E., Cunningham, J. L., and Kenwright, J. (**1998**). "Strain rate and timing of stimulation in mechanical modulation of fracture healing," Clin. Orthop. Rel. Res. **355S**, S105–S115.

Goodship, A. E., and Kenwright, J. (**1985**). "The influence of induced micromovement upon the healing of experimental tibial fractures," J. Bone Joint Surg. **67B**, 650–655.

Harrison, L. J., Cunningham, J. L., Stromberg, L., and Goodship, A. E. (**2003**). "Controlled induction of a pseudarthrosis: A study using a rodent model," J. Orthop. Trauma **17**, 11–21.

Heckman, J. D., Ryaby, J. P., McCabe, J., Frey, J. J., and Kilcoyne, R. F. (**1994**). "Acceleration of tibial fracture-healing by non-invasive, low-intensity pulsed ultrasound," J. Bone Joint Surg. Am. **76**, 26–34.

Hosokawa, A. (**2013**). "Numerical simulations of change in trabecular structure due to bone remodeling under ultrasound propagation," J. Mech. Med. Biol. **13**(1), 1350003.

Isaksson, H., Prantner, V., and Jurvelin, J. S. (**2011a**). "AGE related variation in BMD and trabecular architecture differs between the proximal femur and calcaneus in men," in *ASME 2011 Summer Bioengineering Conference*, Parts A and B, pp. 1079–1080.

Isaksson, H., Rakha, A., Andersson, R., Fredriksson, H., Olsson, J., and Man, P. (**2011b**). "Rye kernel breakfast increases satiety in the afternoon—An effect of food structure," Nutrition J. **10**(1), 10–31.

Kenwright, J., and Gardner, T. (**1998**). "Mechanical influences on tibial fracture healing," Clin. Orthop. Rel. Res. **S355**, S179–S190.

Kristiansen, T. K., Ryaby, J. P., McCabe, J., Frey, J. J., and Roe, L. R. (**1997**). "Accelerated healing of distal radial fractures with the use of specific, low-intensity ultrasound. A multicenter, prospective, randomized, double blind, placebo-controlled study," J. Bone Joint Surg. Am. **79**, 961–973.

Kumagai, K., Takeuchi, R., Ishikawa, H., Yamaguchi, Y., Fujisawa, T., Kuniya, T., Takagawa, S., Muschler, G. F., and Saito, T. (**2012**). "Low-intensity pulsed ultrasound accelerates fracture healing by stimulation of recruitment of both local and circulating osteogenic progenitors," J. Orthopaedic Res. **30**(9), 1–6.

Lacroix, D., Prendergast, P. J., Li, G., and Marsh, D. (**2002**). "Biomechanical model to simulate tissue differentiation and bone regeneration: Application to fracture healing," Med. Biol. Eng. Com. **40**, 14–21.

Leighton, R., Watson, J. T., Giannoudis, P., Papakostidis, C., Harrison, A., and Grant Steen, R. (**2017**). "Healing of fracture non-unions treated with low-intensity pulsed ultrasound (LIPUS): A systematic review and meta-analysis," Injury, Int. J. Care Injured **48**, 1339–1347.

Li, L., Yang, Z., Zhang, H., Chen, W., Chen, M., and Zhu, Z. (**2012**). "Low-intensity pulsed ultrasound regulates proliferation and differentiation of osteoblasts through osteocytes," Biochem. Biophys. Res. Commun. **418**, 296–300.

OReilly, A., Hankenson, K. D., and Kelly, D. J. (**2016**). "A computational model to explore the role of angiogenic impairment on endochondral ossification during fracture healing," Biomech. Model. Mechanobiol. **15**(5), 1–16.

Pauwels, F. (**1941**). "Grundri einer biomechanik der frakturheilung" ("Basic biomechanics of fracture healing"), Biomech. Locomotor Apparatus **34**, 375–407.

Pauwels, F. (**1960**). *Gesammelte Abhandlungen zur Funktionellen Anatomie des Bewegungsapparates* (*Biomechanics of the Locomotor Apparatus*) (Springer-Verlag, New York).

Peiffer, V., Gerisch, A., Vandepitte, D., Van, O. H., and Geris, L. (**2011**). "A hybrid bioregulatory model of angiogenesis during bone fracture healing," Biomech. Model. Mechanobiol. **10**, 383–395.

Perez, M. A., and Prendergast, P. J. (**2007**). "Random-walk models of cell dispersal included in mechanobiological simulations of tissue differentiation," J. Biomech. **40**, 2244–2253.

Pivonka, P., and Dunstan, C. R. (**2012**). "Role of mathematical modeling in bone fracture healing," Bone Rep. **1**, 221.

Prendergast, P. J. (**1997**). "Finite element models in tissue mechanics and orthopaedic implants design," Clin. Biomech. **12**, 343–366.

Protopappas, V., Vavva, M., Fotiadis, D., and Malizos, K. (**2008**). "Ultrasonic monitoring of bone fracture healing," IEEE Trans. Ultras., Ferroelec., Freq. Control **55**, 1243–1255.

Qin, Y.-X., Kaplan, T., Saldanha, A., and Rubin, C. (**2003**). "Fluid pressure gradients, arising from oscillations in intramedullary pressure, is correlated with the formation of bone and inhibition of intracortical porosity," J. Biomech. **36**, 1427–1437.

Shefelbine, S. J., Augat, P., Claes, L., and Simon, U. (**2005**). "Trabecular bone fracture healing simulation with finite element analysis and fuzzy logic," J. Biomech. **38**, 2440–2450.

Tolli, H., Kujala, S., Jamsa, T., and Jalovaara, P. (**2011**). "Reindeer bone extract can heal the critical-size rat femur defect," Int. Orthop. **35**, 615–622.

Vavva, M. G., Grivas, K. N., Aurélie Carlier, A., Polyzos, D., Geris, L., Van Oosterwyck, H., and Fotiadis, D. I. (**2018**). "Effect of ultrasound on bone fracture healing: A computational bioregulatory model," Comput. Biol. Med. **100**, 74–85.

Vetter, A., Witt, F., Sander, O., Duda, G. N., and Weinkamer, R. (**2012**). "The spatio-temporal arrangement of different tissues during bone healing as a result of simple mechanobiological rules," Biomech. Model Mechanobiol. **11**(1–2), 147–160.

Vogelin, E., Jones, N. F., Huang, J. I., Brekke, J. H., and Lieberman, J. R. (**2005**). "Healing of a critical-sized defect in the rat femur with use of a vascularized periosteal flap, a biodegradable matrix, and bone morphogenetic protein," J. Bone Joint Surg.-Am. **87A**, 1323–1331.

Wang, M., Yang, N., and Wang, X. (**2017**). "A review of computational models of bone fracture healing," Med. Biol. Eng. Comput. **55**, 1895–1914.

Wilson, C. J., Schütz, M. A., and Epari, D. R. (**2017**). "Computational simulation of bone fracture healing under inverse dynamisation," Biomech. Model Mechanobiol. **16**, 5–14.

Xu, C., Harris, J. M., and Quan, Y. (**2006**). "Estimating flow properties of porous media with a model for dynamic diffusion," Geoph. Dep., New Orleans, Annual Meeting, pp. 1831–1835.

J. Acoust. Soc. Am. **145** (2), February 2019

Grivas *et al.* 1059